Materials Science Forum
ISSN: 1662-9752, Vol. 1185, pp 29-39
doi:10.4028/p-hr6sOv

Submitted: 2025-12-22
Revised: 2026-02-20
Accepted: 2026-02-23
Online: 2026-04-15

Experimental and Numerical Evaluation of L-PBF Printed Tool for Friction Stir Welding

Zambelli Marco[1,a*], Bocchi Sara[1,b], Negozio Marco[2,c], D'Urso Gianluca[1,d], Giardini Claudio[1,e] and Antonini Laura[1,f]

[1]Department of Management, Information and Production Engineering, University of Bergamo, Via Pasubio 7/b, 24044 Dalmine, BG, Italy

[a]marco.zambelli@unibg.it, [b]sara.bocchi@unibg.it, [c]marco.negozio@unipr.it, [d]gianluca.d-urso@unibg.it, [e]claudio.giardini@unibg.it, [f]laura.antonini@unibg.it

Keywords: friction stir welding, L-PBF, additive manufacturing, AA6082, tool geometry.

Abstract. In Friction Stir Welding (FSW) tool geometry plays a critical role in governing heat generation, material flow, and microstructural evolution within the weld. In this study, the feasibility and performance of FSW tools manufactured by Laser Powder Bed Fusion (L-PBF) are experimentally and numerically investigated. A non-conventional FSW tool produced in AISI 316L by L-PBF was designed and compared with a conventional machined steel tool in the welding of AA6082-T6 sheets performed using already optimized process parameters. This was followed by tensile testing and macro- and micro-hardness measurements, and a punctual microstructural analysis. In addition, a 3D thermo-mechanical finite element model was employed to forecast and analyze the temperature distribution, the effective strain and the overall material flow. The results show that the tool manufactured using L-PBF enables FSW joints to achieve mechanical properties and welding efficiency similar to those of the standard tool. Finite Elements Model (FEM) model, in good agreement with experimental results, show that the geometry of the additive tool promotes greater plastic deformation and lower peak temperatures, confirming both the validity of the model and the suitability of L-PBF for the advanced design of FSW tools.

Introduction

Among solid-state joining methods, Friction Stir Welding (FSW) is considered one of the most efficient, particularly when applied to aluminum alloys [1] [2]. Unlike fusion based processes, such as TIG or MIG/MAG welding, in which the joint region exceeds the melting temperature and undergoes extensive metallurgical transformation, the FSW process is based on the frictional heat generated by a rotating, non-consumable tool to plasticize the material without never reaching its liquid state. The weld efficiency is generally higher than that of TIG without filler metal, and when compared to TIG with filler or MIG/MAG, even though the joint efficiency is sometimes lower, it offers the advantage that drastically reduces distortion, residual stresses, and typical fusion-related defects such as porosity, hot cracking, and embrittlement within the heat-affected zone (HAZ) [3][4]. Welding aluminum alloys can be challenging, and the growing need to join dissimilar alloys [5], often related to cost-saving reasons, adds further complexity to the technology. Also in this scenario, FSW has proven to be more effective than fusion-based processes, as material positioning and process parameters have a decisive influence on joint quality and help avoid many defects typically associated with TIG welding, in which the latter is strongly affected by filler selection, grain growth in the HAZ, and the presence of porosity and micro-voids. In TIG welding, moreover, variations in welding speed can either improve or deteriorate the mechanical properties depending on the selected values, making the process less predictable [6]. Several comparative studies have shown that, even for AA2xxx and AA7xxx that are typically considered the most difficult to weld aluminum alloys, FSW provides superior mechanical properties in every respect compared to other welding techniques [7] [8]. Not only high-strength alloys benefit from the application of the FSW process, but also the AA6xxx series, that are widely used for their good mechanical properties and corrosion resistance. Nevertheless, these properties, the presence of magnesium and silicon makes them particularly sensitive to hot cracking

when fusion temperature is reached. For this reason, conventional welding processes are often improper. This is the reason FSW has shown itself to be an alternative that can be considered reliable, making it possible to create sound joints with detailed microstructure by the process of dynamic recrystallization. Therefore, the FSW method has shown increasing usage in areas that require high-quality welding of aluminum, including the aerospace, automotive, and ship industries. It is essential that a well-designed welding tool be used to create a quality FSW joint, as the tool shape has a direct effect on the material flow and, ultimately, the process stability. The tool is composed of two main elements: the shoulder and the pin, each with its own characteristics and specific tasks. The shoulder remains in contact with the surface of the workpiece, providing most of the frictional heat and confining the plasticized material. Shoulder geometries range from flat and smooth profiles to concave shapes and scroll-type designs, each affecting heat input, downward pressure, and stirring behavior in the upper portion of the weld [9]. The shoulder diameter directly influences the thermal input: larger shoulders generate higher temperatures at the same rotating speed, improving material mixing but also increasing the risk of defects such as excessive flash if the heat becomes excessive.
The pin is responsible for penetrating the material and inducing mechanical stirring within the weld nugget. Its length determines the penetration depth, while its geometry that can be cylindrical, tapered, threaded, or equipped with helical flutes, strongly influences material flow and final microstructural development [10]. Consequently, tool geometry plays a decisive role in determining joint integrity, defect formation, mechanical performance, and microstructural quality.
Complex geometries could enhance the efficiency of the weld joints, concave and grooved shoulders improve material retention and optimized pin designs (threaded, fluted, square), promoting uniform mixing and reducing defects [11]. The fabrication of such geometries is challenging with conventional technologies; however, Additive Manufacturing enables the production of tools with complex shapes. The possibility to create these intricate features and channels improves thermal management, extends tool life, and allows for broad customization without increasing manufacturing complexity [12]. In recent years, increasing attention has been dedicated to the production and maintenance of machining tools through additive manufacturing technologies, particularly Laser Powder Bed Fusion (L-PBF) and Directed Energy Deposition (DED) [13,14]. L-PBF offers high dimensional accuracy, fine microstructures, and the ability to fabricate complex geometries that cannot be produced through conventional machining, especially in the inner part of the tool [15]. These features make L-PBF a promising candidate for manufacturing custom or small-batch FSW tools designed with optimized geometries or internal features.
The production of machining tools, and especially FSW tools, through additive manufacturing has been only partially explored, yet the available results are promising in terms of mechanical performance [16] and the ability to create complex geometries [17].
For these reasons, L-PBF is best suited for rapid prototyping, for the fabrication of special tools, or for experimental contexts where only a limited number of parts with specific functional features are needed. In a traditional industrial setting, however, the high cost of powders and the limited build volume of machines often make the process less economical.
In this context, integrating advanced predictive models becomes essential. Such simulation methods can predict the effects of different tool geometries on the material, reducing prototyping time and cost, and when predictive models reach sufficient accuracy potentially enabling a direct transition to production [18].
For these reasons, the present research involved the design and 3D modeling of a non-conventional FSW tool manufactured using L-PBF. Experimental welds were carried out on AA6082 sheets using both a L-PBF tool and a conventionally turned one, followed by mechanical and microstructural testing. In parallel, welding process simulations were performed using DEFORM-3D software to analyze the heat distribution, material flow, and plastic deformation zones. Finally, the experimental results obtained with the conventional and L-PBF tools were compared with the numerical outcomes to validate the simulation model and assess the compatibility of additive manufactured tools with FSW technology.

The first objective of this study was to determine if and how FSW tools produced by L-PBF are suitable for FSW process of AA6082 and how their performances are compared to conventional tools. A further objective was to assess the extent to which DEFORM-3D simulations can foresee the overall process outcomes, thereby validating the model as a predictive one for advanced FSW application.

Materials and Methods

For the experimental campaign, AA6082-T6 sheets were used as the base material. The plates were arranged in a butt configuration and clamped firmly against a backing plate set at a 3° tilt with respect to the welding direction [19] to promote proper material flow and a stable joint. The first part of the study relied on a standard C40 steel tool, already used in previous work [20] [21].
Once this reference joint was completed, the same welding procedure was repeated using an additively manufactured tool produced by L-PBF, designed with a specific geometry for the purposes of the study (Figure 1). The L-PBF tool was fabricated using gas-atomized AISI 316L powder as the feedstock, which main properties are summarized in Table 1 Printing took place in an inert atmosphere to limit oxidation, considering the parameters listed in Table 1.

Table 1. Properties of the AISI 316 powder and main printing parameters used for manufacturing the L-PBF tool.

LPB-F PRINTING POWDER PROPERTIES									
C	Si	Mn	Cr		Ni		Mo		Fe
<0.03	<1.00	<2.00	Min	Max	Min	Max	Min	Max	Bal.
			16.00	18.00	11.00	14.00	2.00	3.00	

PARTICLE SIZE DISTRIBUTION			**DRYING**
D10	D50	D90	Oven at 70°C for 4 hours (moisture removal)
20.70 µm	34.70 µm	60.60 µm	

PRINTING CONDITIONS					
Layer thickness [µm]	Laser power [W]	Scanning speed [mm/s]	Hatch distance [µm]	Laser spot diameter [µm]	Build plate preheating temperature [°C]
0.30	130	900	80	100	80

Layer spreading was performed using an antistatic polymer recoater, and a stripe scanning strategy was adopted. Between successive layers, the scan direction was rotated by 67° counterclockwise to reduce thermal stress buildup and improve mechanical response. After printing, the tool was detached from the build plate by wire EDM. No heat treatment was needed before it was used for welding.
All the welds, regardless of the considered tool, were performed considering the already optimized process parameters combination for the standard tool, i.e. tool rotational speed (S) of 2400 rpm and feed rate (F) of 375 mm/min [22].

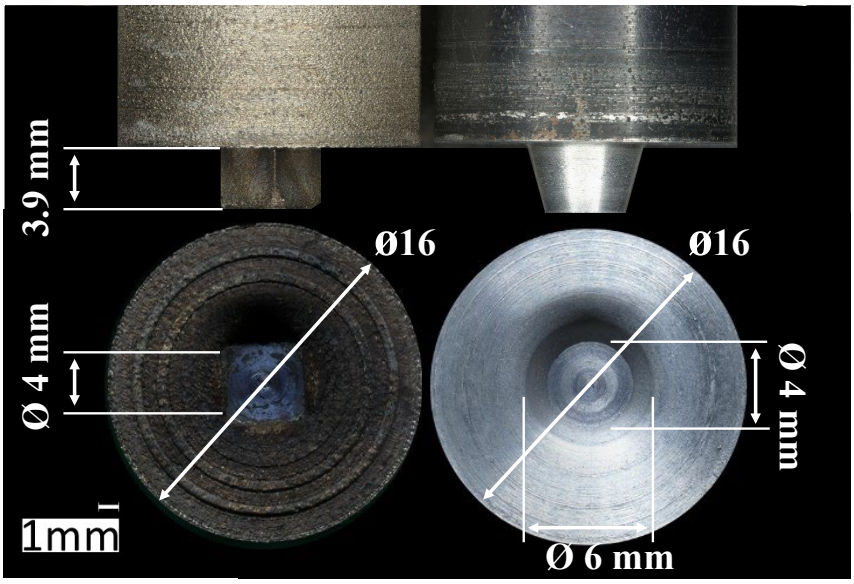

Fig. 1. L-PBF tool (on the left) and Standard tool (on the right). The shoulder of the L-PBF tool has a concave surface with concentric ribs.

For both the welds obtained through the standard and the L-PBF tools, mechanical testing included macro and micro-hardness measurements were performed. Surface hardness was determined using the Rockwell B scale (HRB) following UNI EN ISO 6508. Vickers micro-hardness (HV1000) was measured on cross-sections following a grid layout that satisfies the spacing rules of ASTM EN 92-17, both the hardness patterns are shown in Figure 2.

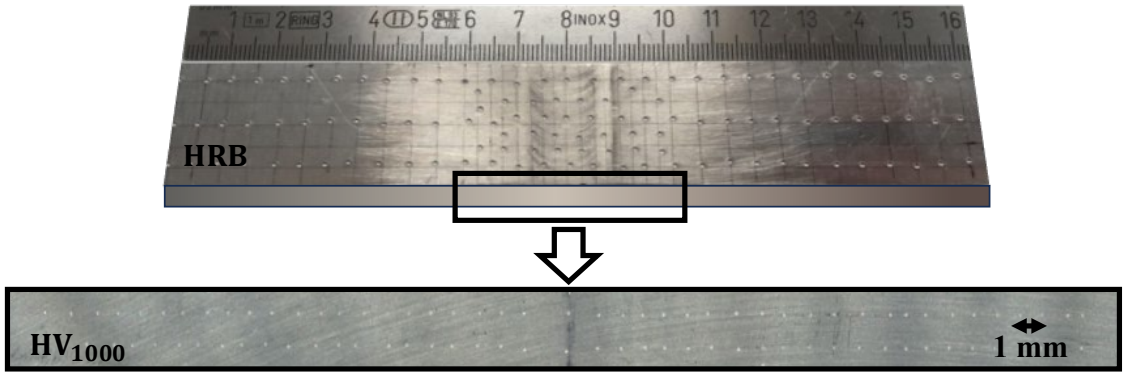

Fig. 2. Distribution of the HRB and HV1000 indentations on the specimen.

Tensile specimens were prepared in line with the geometry set by UNI 10002. Tests were conducted using a Galdabini tensile test machine, with a 0.2 kN preload applied. Two welding samples were tested for each tool. The crosshead speed was fixed at 1.2 mm/min in accordance with UNI EN ISO 6892-1:2019. A MATLAB script was then used to link the applied force acquired by the tensile machine with the measured strain (ϵ_y) and to produce stress-strain curves.

After mechanical testing, the welded joints were sectioned, mounted in resin, and polished with abrasive papers up to 4000 grit, followed by final polishing with 3 μm and 1 μm alumina suspensions. Microstructural features were examined using a digital optical microscope after a double chemical etching. The first etchant consisted of 25 mL HCl (1N), 25 mL HNO_3 (65%), approximately 0.2 mL of HF (50%), and 25 mL methanol (95%); afterward, Weck's reagent was applied.

The grain size measurements were carried out following the Heyn method reported in ASTM E112-13, using the discretization scheme shown in Figure 3.

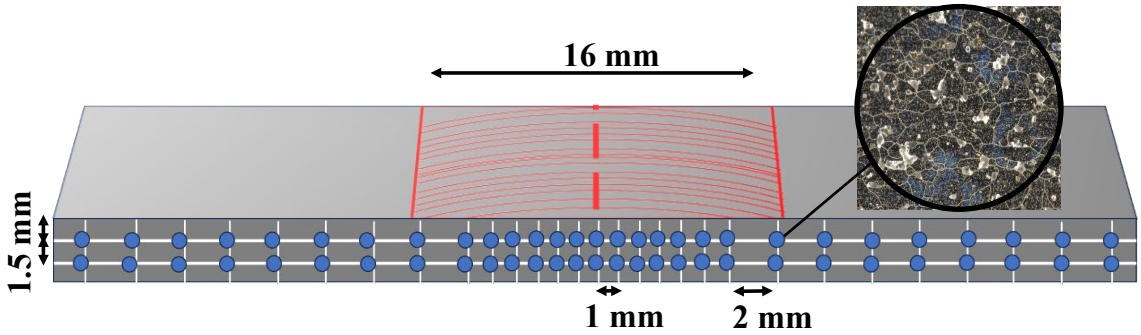

Fig. 3. Microstructures Acquisition Points Using the Optical Microscope.

Using a MATLAB code, a microstructure map of the welded zone was reconstructed, displaying the average transversal grain diameter.

The numerical approach adopted in the present work built directly on a thermo-mechanical simulation model, developed in DEFORM-3D, that has already been validated experimentally in a previous study [18]. The reference model is based on a three-dimensional Lagrangian approach, able to track the local evolution of strain, strain rate, and temperature with good spatial resolution, and it adopts an adaptive remeshing strategy to preserve numerical stability and accuracy, as the large plastic deformation inherent to FSW would otherwise lead to excessive mesh distortion. This strategy involves locally regenerating the mesh in the most highly deformed regions. In the simulation, the tool is assumed to behave as a rigid body, while the workpiece is modeled as a visco-plastic material, where plastic flow clearly dominates over elastic effects. The mechanical response of the material is defined using temperature- strain- and strain-rate-dependent flow curves taken from the DEFORM material database.

Heat generation during welding is accounted for through two contributions: friction at the interface between tool and workpiece and heat produced by plastic deformation in the stirred zone. In this way, the model reproduces the thermal cycles that control microstructural evolution. The boundary conditions governing heat transfer by conduction, convection, and radiation were calibrated using experimental data (Table 2), resulting in simulated temperature profiles that deviate from the measured values by less than 10%, as reported in [23].

Table 2. Calibration parameters for DEFORM simulations.

Parameters	Value
Aluminum Emissivity	0.25
Aluminum Thermal Conductivity $[\frac{N}{(mm \cdot s \cdot °C)}]$	450
Friction Coefficient Aluminum-Steel	0.6
Heat Transfer Coefficient Aluminum-Steel $[\frac{N}{(mm \cdot s \cdot °C)}]$	11
Heat Exchange with the Environment $[\frac{N}{(mm \cdot s \cdot °C)}]$	0.02
Mechanical Conversion to Heat	0.8

The thermo-mechanical simulation ultimately provides the complete history of effective strain, strain rate, and temperature at each material point and the same model was used considering fixed process parameters (S2400 rpm and F375) and by changing the geometry of the tool, in order to compare the obtained results also from the simulation point of view.

Results

The welds have a visually satisfying overall appearance, with consistent and clearly defined bead morphology in all conditions. No macro-defects were observed in any of the joints, including tunnel voids, lack of penetration, or root defects.

The graphs reported in Figure 4 show the hardness distribution along the transverse cross-section of the FSW joint, evaluated in terms of both Rockwell B macro-hardness (HRB) and Vickers micro-hardness (HV1000), as a function of the distance from the weld center.

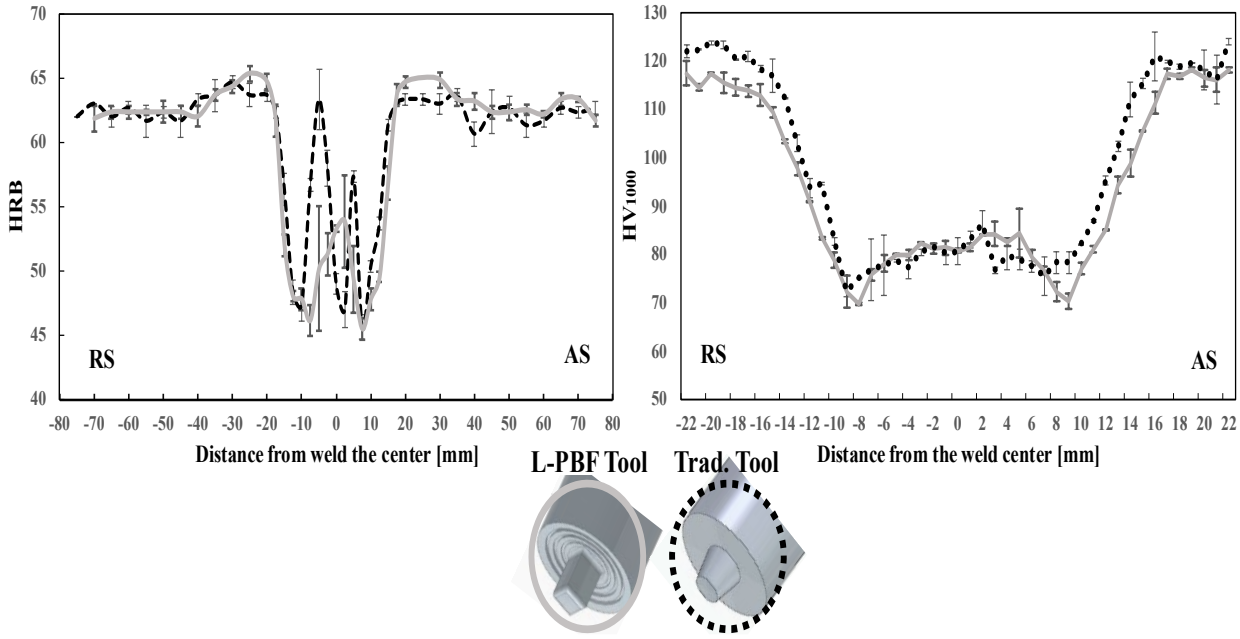

Fig. 4. HRB and HV1000 Hardness Comparison Charts, L-PBF Tool Compared with Traditional Tool at F375 S2400.

In both cases, the typical W-shaped profile associated with the FSW process is observed. Hardness shows its maximum in the base material, gradually decreases when approaching the welded zone, and attains a minimum near the transition between the nugget and the TMAZ, before increasing almost symmetrically on the opposite side of the joint. The HRB profile clearly highlights, for both the geometries of the tool, a localized softening region around the center of the joint, with minimum hardness values that vary depending on the tool configuration. The differences observed among the profiles suggest that tool geometry affects less the extent and more the severity of the softening, likely through variations in heat generation and material flow. In particular, The L-PBF tool shows minimum hardness values comparable to those of the conventional tool, however, on average, it exhibits lower hardness in the nugget and TMAZ regions, following a more uniform hardness trend. The HV1000 micro-hardness profile confirms the hardness reduction in the central region of the joint, even if it is evidently more gradual and directly reflects local microstructural modifications, particularly grain size and precipitate condition. The recovery of hardness toward the base material is symmetric, indicating that the observed variations are mainly governed by the thermal field rather than by macroscopic welding defects. In this case, it can be stated that the hardness curves obtained using the conventional tool and the L-PBF tool are practically overlapped.

The tensile test results (Figure 5) obtained using the L-PBF tool show a very consistent mechanical response. The two stress–strain curves exhibit similar trends, with only minor variations in ultimate tensile strength (UTS). This limited UTS variation is a positive indicator of good process repeatability and highlights the stability of the welding conditions, regardless the considered tool geometry.

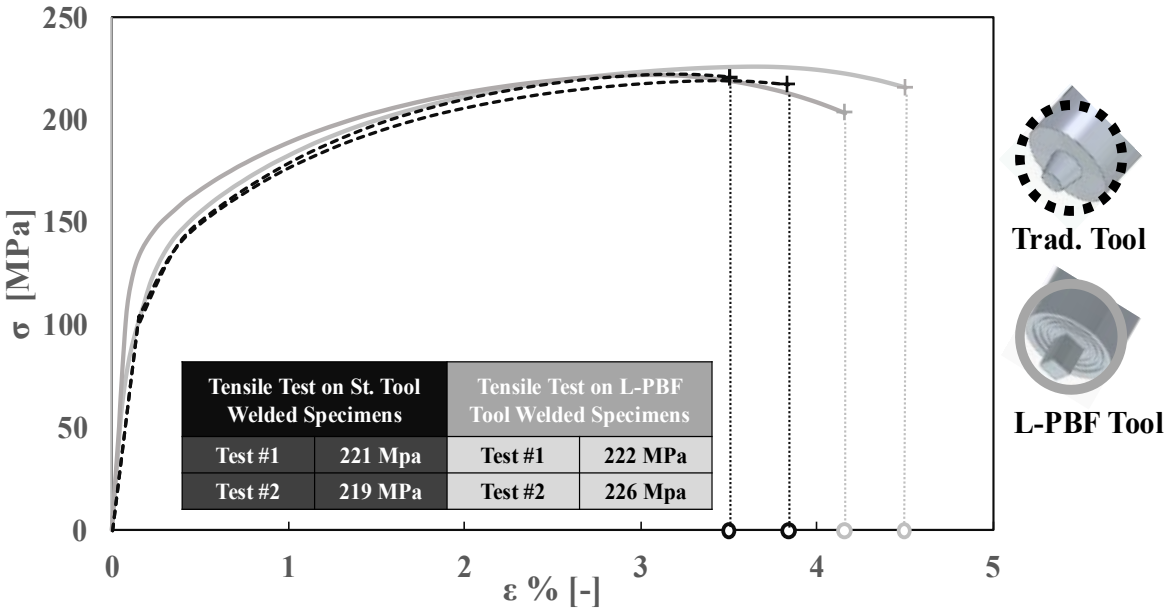

Fig. 5. Tensile Test curves of: L-PBF Tool compared with Standard Tool at S2400 F375.

When compared with the reference values obtained using the standard Tool, the UTS achieved with the L-PBF tool is fully comparable, indicating that the adoption of an additively manufactured tool does not adversely affect joint strength. The welding efficiency is approximately 68%, with minor variations observed between joints produced using the traditional tool and those welded with the L-PBF tool. Overall, the tensile results confirm that the L-PBF tool is capable of producing sound and repeatable joints with mechanical performance comparable to that obtained using the standard one.
The FSW process is inherently a thermomechanical process, in which it is important to evaluate the mechanical characteristics of the obtained welds, but it is equally important to analyze how the deformations and heat flow generated by the process are distributed in the material being processed. This is because these characteristics also risk significantly affect the tool wear, reducing the useful life of the tool, leading to pin deformation and thus affecting the quality of the weld. For this reason, the responses of the simulation model in terms of effective strain and temperature were analyzed.
The images show the responses of the numerical model in terms of effective strain (Figure 6) and temperature (Figure 7), allowing a direct comparison between the square tool made using L-PBF and the standard tool.

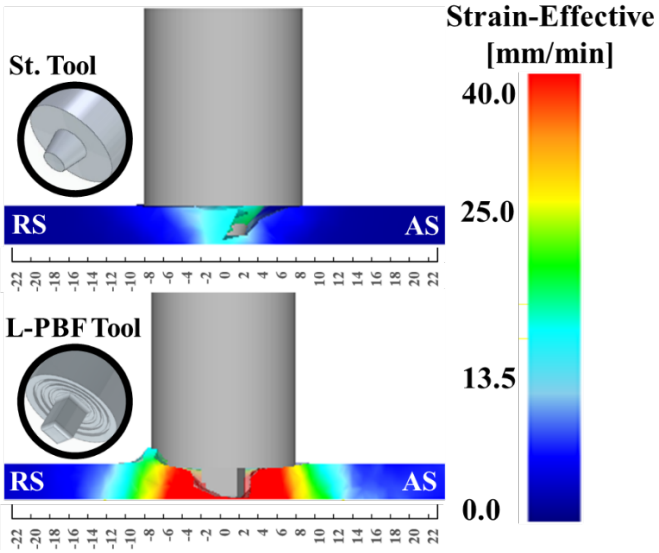

Fig. 6. DEFORM simulation results for effective strain: standard tool compared with L-PBF one.

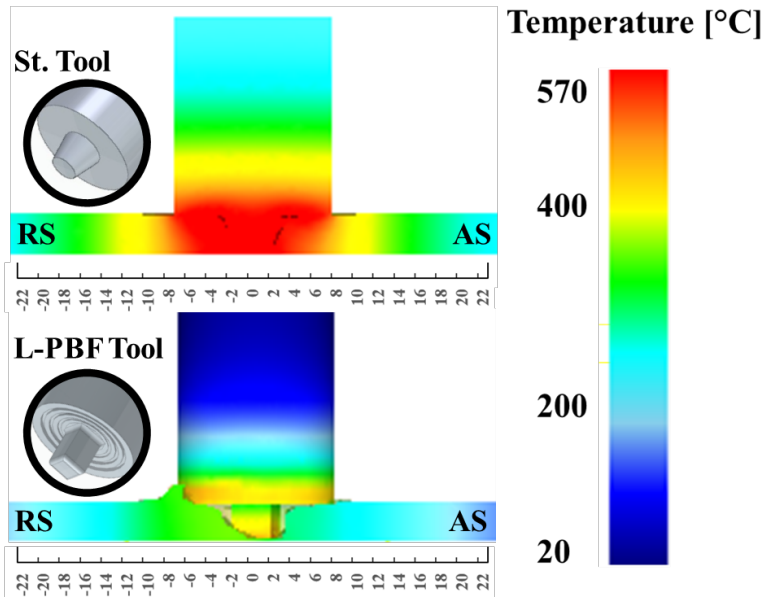

Fig. 7. DEFORM simulation results for temperature: standard tool compared with L-PBF one.

The effective strain maps clearly show that, in the case of the square tool (Figure 6), the weld is characterized by significantly higher levels of plastic deformation, strongly concentrated in the area along the tool-workpiece interface. This behavior indicates greater mechanical stirring action, favored by the non-axially symmetric geometry of the pin, which increases material mixing and the severity of local deformations. In the case of the standard tool (Figure 6), on the contrary, the deformations are lower and more distributed, suggesting a less marked mechanical contribution to the welding process. This difference highlights how the geometry of the tool plays a decisive role in balancing the mechanical and thermal components of the FSW process.

Opposing considerations emerge from the analysis of the temperature maps (Figure 7). In the case of the standard tool (Figure 7), both the tool and the welded material are subjected to more intense thermal cycles, with higher temperatures and more pronounced thermal gradients in the process zone. This indicates a greater incidence of heat generated by friction, which becomes the dominant component of the process.

In the square tool model (Figure 7), on the other hand, the maximum temperatures are lower overall. This suggests that a greater proportion of the energy introduced is dissipated in the form of plastic deformation rather than heat, reducing the extent of the thermal cycles to which both the workpiece and the tool are subjected.

Overall, the images confirm that the square tool tends to promote the mechanical component of FSW, while the standard tool stresses the thermal component of the process. Both approaches have advantages and critical issues: high deformations can improve mixing but accelerate wear or deformation of the pin and more severe thermal cycles can negatively affect the microstructure of the joint and contribute to thermal degradation of the tool.

The same conclusions can be drawn by examining the results obtained experimentally from the measurements of the average grain diameters in the different zones characterizing the FSW joint. From a microstructural point of view (Figure 8), this results into a stir zone characterized by fine, homogeneous grains, which are more extensive in the case of the square tool than in the standard tool.

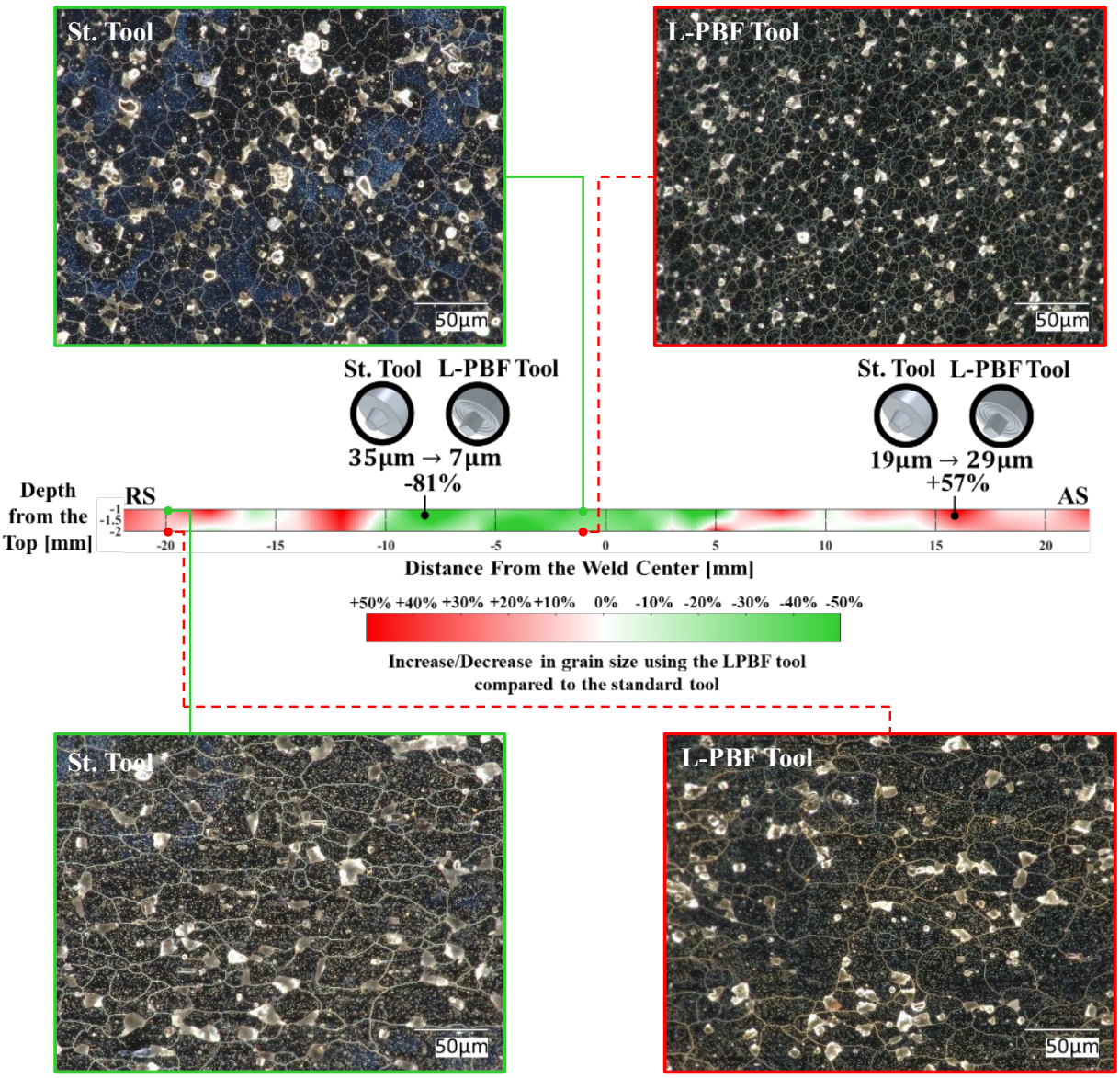

Fig. 8. Increase/Decrease in Grain Size Using the LPBF Tool Compared to the Standard Tool.

The average reduction in grain size within the region comprising the nugget and the TMAZ is approximately 33%, with the crystalline microstructure remaining, on average, finer up to about 16 mm from the weld center.

The high mechanical component of the FSW process associated with the square tool, highlighted by the higher effective strain values, promotes intense plastic deformation and dynamic recrystallization phenomena, which are responsible for refining the microstructure and enlarging the area of effectively remixed material. In the case of the standard tool, on the contrary, the greater incidence of the thermal contribution leads to a more limited central zone, in which grain refinement is less extensive, as the process is governed more by friction heating than by severe plastic deformation.

Conclusion

In this work, the feasibility of using additively manufactured Friction Stir Welding tools produced by Laser Powder Bed Fusion was investigated through a combined experimental and numerical approach. Experimental welding trials on AA6082-T6 sheets demonstrated that the L-PBF tool is capable of producing sound joints with no macroscopic defects and with mechanical properties fully comparable to those obtained using a conventional, machined tool. Hardness distribution and tensile test results proved a similar welding efficiency and weld quality between these two tool arrangements.

Numerical simulation results had offered a great benefit in understanding the thermo-mechanical process characteristics and the effect of tool geometry. It had been demonstrated that the tool geometry designed using L-PBF indicated an enhanced degree of plastic deformation with lower maximum temperatures than with the conventional tool; therefore, there was an apparent change in the relative contributions from the mechanical stirring component and the friction component. This difference had resulted in variations in both the predicted grain structure and its homogeneity.
The good agreement between experimental data and simulation results proves the correctness of the simulation model selected for the simulation and the effectiveness of the L-PBF process for FSW tool production. In summary, the obtained results have shown to confirm the effectiveness of the L-PBF process for manufacturing FSW tools and have underlined the potential of this process for future industrial applications. Furthermore, the integration of experimental testing with advanced numerical modeling proves to be a powerful approach for supporting the design, optimization, and future development of innovative FSW tool geometries.

References

[1] M.I.A. Habba, M.M.Z. Ahmed, Friction stir welding-based technologies: A comprehensive review from the sustainable manufacturing perspectives, Journal of Materials Research and Technology, 38 (2025) 1–29.

[2] Neeru Bhardaj, Uday Dixit, et al., Recent Developments in Friction Stir Welding and Resulting Industrial Practices, Research Gate, (2019).

[3] B. Yelamasetti, M. Sridevi, N.S. Sree, N.K. Geetha, P. Bridjesh, S.D. Shelare, C. Prakash, Comparative Studies on Mechanical Properties and Microstructural Changes of AA5052 and AA6082 Dissimilar Weldments Developed by TIG, MIG, and FSW Techniques, Journal of Materials Engineering and Performance 2024 34:11, 34 (2024) 9972–9985.

[4] A.P. Reddy, S. Dewangan, A COMPARATIVE ANALYSIS AMONG THE WELDED Al-6061 PLATES JOINED BY FSW, MIG AND TIG WELDING METHODS, 29 (2023) 75–81.

[5] S. Sambasivam, N. Gupta, A. saeed jassim, D. Pratap Singh, S. Kumar, J.M. Giri, M. Gupta, A review paper of FSW on dissimilar materials using aluminum, Mater Today Proc, (2023).

[6] S. Mabuwa, V. Msomi, Review on Friction Stir Processed TIG and Friction Stir Welded Dissimilar Alloy Joints, Metals 2020, Vol. 10, Page 142, 10 (2020) 142.

[7] Aydın ŞIK, M. Önder, Comparison between mechanical properties and joint performance of AA 2024-O aluminium alloy welded by friction stir welding and TIG processes, Kovove Materialy-Metallic Materials, (2012).

[8] U. Dwivedi, S. Tiwari, A. Mishra, S. Das, Comparative Study of Weld Characteristics of Friction Stir Welded Joints on Aluminium 7075 with Autogenous TIG, Mater Today Proc, 22 (2020) 2532–2538.

[9] Evaluation of Friction Stir Weld Process and Properties for Aircraft Applications, 2018.

[10] TWI - Designs and Materials of Friction Stir Welding Tools, (2024).

[11] Y.N. Zhang, X. Cao, S. Larose, P. Wanjara, Review of tools for friction stir welding and processing, Canadian Metallurgical Quarterly, 51 (2012) 250–261.

[12] M. Xing, H. Wang, Z. Zhao, H. Lu, C. Liu, L. Lin, M. Wang, X. Song, Additive manufacturing of cemented carbides inserts with high mechanical performance, Materials Science and Engineering: A, 861 (2022) 144350.

[13] Victor Lubkowitz, Nitin Reothia, Frederik Zanger, Enhancement of groove turning performance by additively manufactured tool holders with internal cooling channels and combined cooling strategies, 21st Machining Innovations Conference for Aerospace Industry 2021, (2021).

[14] M. Seyam, P. Koshy, M. Elbestawi, Laser powder bed fusion of WC-Co form turning tools with integrated cooling features: Design, printing, and test machining of Ti6Al4V, CIRP Annals, 73 (2024) 65–68.

[15] S. Gruber, C. Grunert, M. Riede, E. López, A. Marquardt, F. Brueckner, C. Leyens, Comparison of dimensional accuracy and tolerances of powder bed based and nozzle based additive manufacturing processes, J Laser Appl, 32 (2020) 32016.

[16] A. Alshami, A. Shuaib, A. Mayyas, Evaluation of the properties of experimental friction stir welding pin tools consolidated from W-25 wt% Re alloy using laser powder bed fusion (LPBF) process, Manuf Lett, 44 (2025) 1038–1043.

[17] M. Seyam, P. Koshy, M. Elbestawi, Laser powder bed fusion of WC-Co form turning tools with integrated cooling features: Design, printing, and test machining of Ti6Al4V, CIRP Annals, 73 (2024) 65–68.

[18] S. Bocchi, M. Negozio, Experimental Investigation and Finite Element Simulation of the Microstructural Evolution in AA6082 Friction Stir Welded Joints, J Mater Eng Perform, 34 (2025) 11274–11291.

[19] S. Bocchi, G. D'Urso, C. Giardini, The effect of heat generated on mechanical properties of friction stir welded aluminum alloys, The International Journal of Advanced Manufacturing Technology, 112 (2021) 1513–1528.

[20] S. Bocchi, G. D'Urso, C. Giardini, Influence of copper interlayer on the mechanical performance of friction stir welded AA2024, International Journal of Advanced Manufacturing Technology, 133 (2024) 5811–5828.

[21] S. Bocchi, G. D'urso, C. Giardini, Preliminary study of the mechanical characteristics implementation of friction stir welded AA2024 joints by adding pure copper, Materials Research Proceedings, 25 (2023) 213–220.

[22] M. Quarto, S. Bocchi, G. D', N.A. Urso, C. Giardini, Hybrid finite elements method-artificial neural network approach for hardness prediction of AA6082 friction stir welded joints, International Journal of Mechatronics and Manufacturing Systems, 15 (2022) 149.

[23] S. Bocchi, M. Negozio, Experimental Investigation and Finite Element Simulation of the Microstructural Evolution in AA6082 Friction Stir Welded Joints, (n.d.).